Electrochimica Acta 53 (2008) 6337–6343

Contents lists available at ScienceDirect

Electrochimica Acta

journal homepage: www.elsevier.com/locate/electacta

Water removal from a PEFC during gas purge

Kazuya Tajiri [a], Chao-Yang Wang [a,*], Yuichiro Tabuchi [b]

[a] Electrochemical Engine Center (ECEC), Department of Mechanical and Nuclear Engineering, The Pennsylvania State University, University Park, PA 16802 USA
[b] Nissan Motor Co. Ltd., Nissan Research Center, Kanagawa 237-8523, Japan

ARTICLE INFO

Article history:
Received 4 March 2008
Received in revised form 12 April 2008
Accepted 13 April 2008
Available online 22 April 2008

Keywords:
Automotive fuel cells
Gas purge
Water removal
High-frequency resistance
Experimental

ABSTRACT

Gas purge intended to minimize residual water in a polymer electrolyte fuel cell (PEFC) during shutdown is critically important for cell performance and durability under freeze/thaw and cold-start cycling. This paper presents an experimental study of short-duration gas purge relevant to automotive application. A novel experimental procedure has been devised to achieve excellent reproducibility and consistency of purge data. Using the high-frequency resistance (HFR) of the cell as an indicator of membrane water content and hence of purge effectiveness, it is found that the purge performance can be uniquely described by two characteristic parameters, one representing the diffusive flux of water vapor across the catalyst layer and gas diffusion layer, and the other standing for the convective flux of water vapor down the channel with purge gas. A large set of purge data obtained over a range of purge cell temperature, purge gas flowrate and relative humidity and for two purge gases (N_2 and He) have been organized as function of these two parameters. Due to its threefold higher water diffusivity, Helium gas purge is seen to be superior over N_2, particularly under purge conditions controlled by through-plane vapor diffusion such as lower purge temperatures and shorter purge durations. It is also shown that the HFR after purge typically decreases in a time scale of 1–2 h and that the extent of HFR relaxation generally increases with higher HFR or lower membrane water content after purge.

1. Introduction

Gas purge is an integral part of the frequent shutdown process of polymer electrolyte fuel cells (PEFC) as a fuel cell vehicle (FCV) typically goes through a large number of start and stop cycles. In some situations, gas purge serves to avoid or minimize various types of material degradation in a fuel cell stack, some of which are permanent and catastrophic. In others, gas purge is intended to remove water from the fuel cell, thus avoiding ice formation and blockage when exposed to sub-freezing temperatures.

Much research has reported the possible carbon corrosion on the air electrode due to residual hydrogen in the anode during idle state. This degradation is primarily caused by the presence of a H_2/O_2 front in the anode along with the high cathode voltage (~open circuit voltage), and can be prevented by fully removing the hydrogen from the anode compartment. Lee et al. studied the effect of the residual hydrogen in the anode compartment during the idle using polarization measurement, cyclic voltammetry and electron microscopy, and found that hydrogen removal from the anode channels by gas purge helps prevent fuel cell degradation [1].

In the cathode side, on the other hand, the primary purpose of gas purge is to remove water from the cathode compartment, particularly in preparation for cold start from subzero temperatures. As gas purge defines the initial condition of water distribution in a cell, it is a crucial step in the PEFC cold start. Recent experimental studies have amply shown that not only performance but also material durability of PEFC hinges strongly upon the gas purge process prior to cool-down and cold start [2–6]. This is because an effective gas purge can remove water from the catalyst layer and membrane, thereby creating space for water produced in cold start to be stored.

Tajiri et al. [7,8] developed a method of equilibrium purge, in which a cell is purged with partially humidified gas for an extended period of time (typically 3 h or more) so as to remove all the liquid water in the cell as well as to equilibrate the proton exchange membrane and ionomer in the catalyst layer (CL) with the purge gas relative humidity (RH). The distribution of water in the cell is well controlled in equilibrium purge, thus providing an excellent experimental technique for fundamental research of PEFC cold start and other problems requiring highly reproducible gas purge practice. Whereas the equilibrium purge is useful for laboratory experiments, practical gas purge for FCVs requires much shorter duration, preferably less than 60 s, and high efficiency. Therefore, a

* Corresponding author. Tel.: +1 814 863 4762; fax: +1 814 863 4848.
E-mail address: cxw31@psu.edu (C.-Y. Wang).

0013-4686/$ – see front matter © 2008 Elsevier Ltd. All rights reserved.
doi:10.1016/j.electacta.2008.04.035

fundamental understanding of water removal during practical gas purge is necessary. Unfortunately, very little is known in the literature on purge mechanisms for automotive application. St-Pierre et al. [9] showed that cool purge at 20 °C is better than hot purge at 85 °C. Performance losses were not observed in a cell purged with dry gas at 20 °C after the freeze/thaw cycling. Bradean et al. [10] touched upon the purge effectiveness using one section of their paper to briefly present a one-dimensional model and experimental results, and concluded that the purge cell temperature is the most critical parameter for an effective purge. However, they did not seek a fundamental understanding of purge mechanisms.

Ge and Wang [11] measured the cell high-frequency resistance (HFR) during gas purge with various purge durations, and demonstrated that the cell HFR directly impacts the amount of product water generated or cell operational time in isothermal cold start. Sinha et al. [12] used X-ray microtomography to dynamically visualize the liquid water in the gas diffusion layer (GDL) and calculated the variation of liquid saturation with time during room-temperature purge. St-Pierre et al. [13] developed a residence time distribution method and demonstrated its potential to detect liquid water in gas channels and electrodes. Most recently, Sinha and Wang [14] presented a comprehensive theoretical description of water removal phenomena during gas purge, classifying the process into four stages, through-, in-plane drying, vapor transport and membrane equilibrium stages. The theoretical predictions further concluded that the high cell temperature and low RH and high flow rate of purge gas facilitates water removal.

The present work concerns experimental characterization of gas purge typical of automotive applications. In the next section, we describe a new experimental method, setup, and procedure to characterize gas purge of short duration. Much attention has been paid to finding a procedure to achieve reproducible purge experiments. A purge curve is defined and stages of gas purge are elaborated. Then, we introduce two characteristic parameters to describe the purge performance. Finally, we present a comprehensive set of experimental results characterizing automotive gas purge for the first time.

2. Experimental methods

We note that the purpose of gas purge is not to address how much water is removed from the cell, or how thoroughly the GDL is dried. Instead, gas purge is ultimately to remove water from the catalyst layer and membrane, thereby creating space for water produced in cold start to be stored. Thus, we propose to use the membrane HFR (or more conveniently cell HFR) as the indicator to measure effectiveness of gas purge. A purge curve is thus defined as the cell HFR versus purge time in this work. An effective purge protocol is the one that reaches a certain HFR within the shortest purge time (with least energy consumption as well).

2.1. Experimental setup

The fuel cell used in this study has straight, parallel flow channels with the dimensions of 54-mm length, 1-mm width, 0.6-mm depth, and 1-mm land width. The number of channels is 24, with total active area of 25 cm^2. The membrane electrode assemblies (MEAs) used are commercially available from JAPAN GORE TEX INC. with 30-μm thick membrane and catalyst layer of 0.4 mg/cm^2 Pt on each electrode. Toray carbon paper coated with a microporous layer (MPL) was used as the GDL.

The fuel cell discharge and gas purge operation is carried out and controlled by a fuel cell test station (Arbin Instruments, College Station, TX), and the cell temperature is controlled with a heat transfer fluid passing through the coolant channels located in the stainless steel end plates. During gas purge, the cell HFR is measured at 1 kHz using an AC milliohm meter (Tsuruga model 3566, Osaka, Japan).

2.2. Experimental procedure

The practical, short-duration gas purge of a fuel cell is inherently transient and extremely sensitive to the initial water distribution inside the cell. Therefore, controlling the initial conditions prior to gas purge is of paramount importance to ensure reproducibility and consistency of purge results. Extreme care must be taken to establish a controllable pre-purge condition and demonstrate the repeatability of purge data. Our procedure, after extensive trial-and-error, is described below.

First, the fuel cell is operated at a discharge current density of 0.5 A/cm^2 for 1 h with fully humidified H_2 and air at 30 °C. This step is to ensure that the membrane is identically in the fully hydrated state in all experiments. Then, an equilibrium purge is carried out for the cell, that is, the cell is purged with partially humidified nitrogen for a sufficiently long period (typically 3–4 h). In this study the cell temperature is fixed at 35 °C while the purge gas dew point is controlled at 30 °C, which corresponds to 75% relative humidity. At the end of this step liquid water in the cell is expected to be completely removed and the membrane is in equilibrium with the 75% RH gas. At this point it is assumed that all the history of the cell is totally erased and the cell is in the identical condition of every experiment.

The next step is to create a controllable pre-purge condition by mimicking the FCV situations prior to shutdown and gas purge, that is, to generate some liquid water in the cell. By changing operating conditions of this step, it is possible to control the amount of liquid water in the cell. In the present study, we discharge the cell at 0.5 A/cm^2 for 10 min with cell temperature of 55 °C and stoichiometry of 18 and 21.6 for H_2 and air, respectively, both fully humidified and at ambient pressure. Although we cannot quantify the amount of liquid water present in the cell prior to purge, we can reproduce the same initial condition under which a comparative study becomes possible.

Then, the cell is gas-purged under various conditions to be described in detail in the next section. In all cases, gas purge was conducted on both anode and cathode sides without circulation. Once a gas purge is completed, the valves at the cell inlet and outlet are closed and the cell temperature is maintained constant to monitor any HFR change after purge. The membrane HFR typically decreases over the time scale of one to 2 h, a phenomenon called HFR relaxation after purge in this work.

2.3. Two characteristic parameters for water removal

To better analyze and understand gas purge, we propose two characteristic parameters based on a simplified schematic of purge physics, as shown in Fig. 1. Although the figure only shows the cathode side of the fuel cell from the polymer electrolyte membrane to the gas channel, the same conceptual depiction is applicable to the anode side. Prior to gas purge, CL and GDL are partially saturated with liquid water. We assume that water removal during gas purge is primarily a vapor-phase transport process, because liquid water residing in gas channels is swept away typically within the very first seconds of purge operation and the liquid water motion inside CL and GDL is sufficiently slow to be considered quasi-stationary in the time scale of a gas purge. Thus, the water is removed from the liquid surfaces residing within CL/GDL to the gas channel by through-plane vapor diffusion. Subsequently, the water is removed by the down-the-channel convection by purge gas. Mathematically,

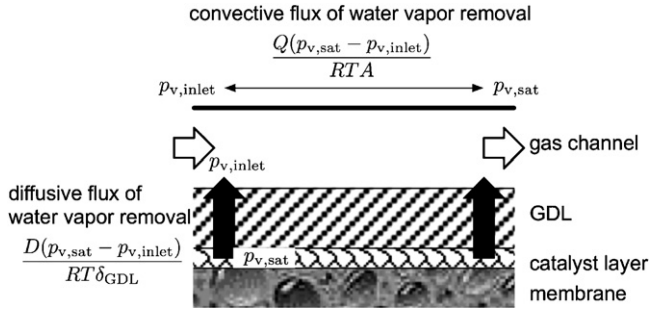

Fig. 1. Schematic diagram of two limiting stages of water removal during gas purge.

the first process of water vapor removal can be characterized by the through-plane diffusive flux between a liquid surface in CL/GDL to the gas channel, i.e. $D(p_{v,sat}-p_{v,inlet})/RT/\delta_{GDL}$. Here D stands for the diffusion coefficient of water in purge gas, and $p_{v,sat}$ and $p_{v,inlet}$ the saturation vapor pressure at the purge temperature and the water vapor partial pressure in the purge gas at the inlet, respectively. R is the universal gas constant, T the purge cell temperature, and δ_{GDL} an effective diffusion length for water vapor from the membrane surface to the gas channel, which should scale mainly with the GDL thickness but could also contain effects of CL and MPL thickness and porosity, as well as the effects of the land-to-channel width ratio to account for in-plane transport effects.

The second process of water vapor removal down the channel can be described by the convective flux, $Q(p_{v,sat}-p_{v,inlet})/RT/A$, representing the maximum amount of water vapor removed with the purge gas when the exit purge gas is fully saturated with vapor. In the above definition Q is the purge gas volumetric flow rate and A the active area of the fuel cell. Both parameters defined above have the unit of mol/s per unit of the fuel cell active area. It follows that the net rate of water removal during gas purge is determined by the two characteristic parameters and their relative magnitudes.

To study the effects of these characteristic parameters as well as the direct operating parameters, such as the purge cell temperature and purge gas flow rate, we have taken the following approach in carrying out experiments.

To examine the effect of the vapor diffusion coefficient D, N_2 and He are used as the purge gas in this study. The diffusion coefficient of water vapor in He is roughly three times that in N_2. While impractical for vehicle application, He gas is used here solely as a diagnostic tool.

The purge gas RH in the vast majority of our experiments has been controlled at higher than 40% in order to avoid the regime of very low membrane water content where there is a large uncertainty in our knowledge of the membrane behavior.

The duration of gas purge is 60 s in most experiments (except Section 3.1), and experimental data include the profiles of HFR evolution with time during purge and the final HFR values at the end of purge.

All purge conditions in this study are tabulated in Table 1 along with the calculated two characteristic parameters. Two purge gases, N_2 and He, are used with four different flow rates for N_2 (1.0, 3.0, 4.5, and 9.0 L/min) and two flow rates for He (1.0 and 4.5 L/min). The cell temperatures at purge are 42, 55, and 75 °C, respectively, and for all temperatures the RH of the purge gas is controlled at no less than 40% based on the purge cell temperature. Case 1, for example, yields a diffusive flux and a convective flux of 2.96×10^{-5} mol/(cm^2 s) and 1.43×10^{-6} mol/(cm^2 s), respectively, using the following parameters: $D = 0.318$ cm^2/s, $p_{v,sat} = 8132$ Pa, $p_{v,inlet} = 3253$ Pa, $T = 315.2$ K, $\delta_{GDL} = 0.02$ cm, $Q = 19.2$ cm^2/s (=1 L/min at 0 °C), and $A = 25$ cm^2.

Furthermore, because the cell HFR or membrane proton conductivity is also a function of temperature, we convert the raw HFR data at different purge temperatures to the single reference temperature of 30 °C via the following temperature-dependent correlation obtained from separate in situ measurements:

$$\text{T-compensated HFR} = \exp\left[1455\left(\frac{1}{303}-\frac{1}{T}\right)\right]\text{HFR}_{\text{purge}} \quad (1)$$

The temperature-compensated HFR is then essentially indicative of membrane water content only, and the temperature dependence is removed from actually measured HFR data. All HFR results shown in the following sections are the T-compensated values, unless otherwise noted.

3. Results and discussion

3.1. Verification of repeatability

As explained earlier, realizing consistent and reproducible purge experiments is a critical step towards the development of a reliable purge database and hence a fundamental understanding of purge mechanisms. Here, we verify the experimental repeatability through multiple purge experiments of various duration performed under identical purge conditions. Fig. 2 shows the time evolution of cell HFR during gas purge for four experiments with different purge duration. The purge cell temperature is 55 °C and the purge gas is dry N_2 with the flow rate of 4.5 L/min. We use the dry purge gas in this set of experiments, unlike all other experiments of this study, in order to provide the most severe condition to verify the experimental repeatability. It should also be mentioned that the cell HFR shown in this figure is not compensated for temperature, but raw data at the cell temperature of 55 °C. The excellent repeatability is evident by the fact that purge curves of longer duration closely overlap those of short durations, under otherwise identical purge conditions. We recommend that the type of repeatability tests as shown in Fig. 2 be carried out as a standard procedure in all purge experiments before reporting meaningful results.

Table 1
Purge conditions and HFR values after 60 s of purge

Case#	1	2	3	4	5	6	7	8	9	10	11	12	13	14	15	16	17	18	19	20
Cell temperature (°C)	42	55	75	42	55	75	42	55	75	42	55	75	42	55	75	42	55	75	42	55
Purge gas dew point (°C)	26	37	55	26	37	55	26	37	55	26	37	55	26	37	55	26	37	55	26	37
Purge gas relative humidity (%)	40	40	40	40	40	40	40	40	40	40	40	40	40	40	40	40	40	40	40	40
Purge gas flow rate (at 0 °C) (L/min)	1	1	1	3	3	3	4.5	4.5	4.5	9	9	9	1	1	1	4.5	4.5	4.5	2	2.5
Purge gas species	N_2	N_2	N_2	N_2	N_2	N_2	N_2	N_2	N_2	N_2	N_2	N_2	He	He	He	He	He	He	He	He
Diffusive flux of water vapor removal ($\times 10^5$ mol/(cm^2 s))	2.96	5.85	14.74	2.96	5.85	14.74	2.96	5.85	14.74	2.96	5.85	14.74	9.19	18.12	45.68	9.19	18.12	45.68	9.19	18.12
Convective flux of water vapor removal ($\times 10^6$ mol/(cm^2 s))	1.43	2.77	6.78	4.30	8.31	20.33	6.45	12.46	30.49	12.89	24.92	60.98	1.43	2.77	6.78	6.45	12.46	30.49	2.86	6.92
Post-purge HFR (mΩ cm^2)	115	245	290	206	301	327	223	336	317	291	410	340	252	335	306	361	399	366	305	383
T-compensated HFR (mΩ cm^2)	138	353	540	247	434	608	268	484	590	349	591	633	303	483	569	433	575	681	366	552
Relaxed HFR (mΩ cm^2)	100	127	151	124	137	175	118	157	143	134	135	180	130	165	148	160	173	210	131	143
T-compensated relaxed HFR (mΩ cm^2)	120	183	281	149	198	326	142	226	266	161	195	335	156	238	276	192	249	391	157	206

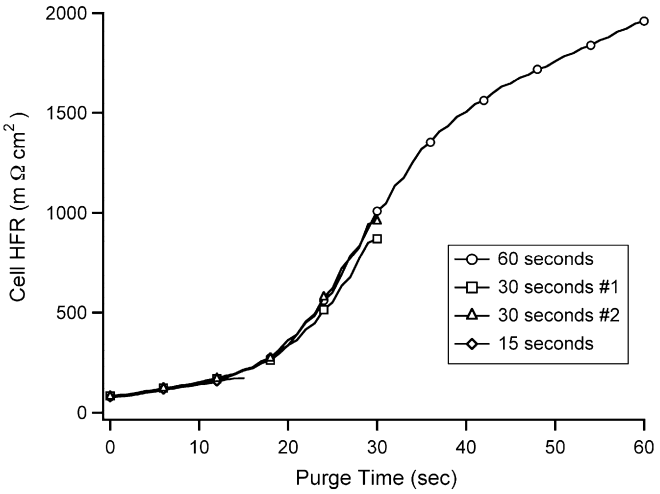

Fig. 2. Time evolution of cell HFR for four experiments with different purge durations.

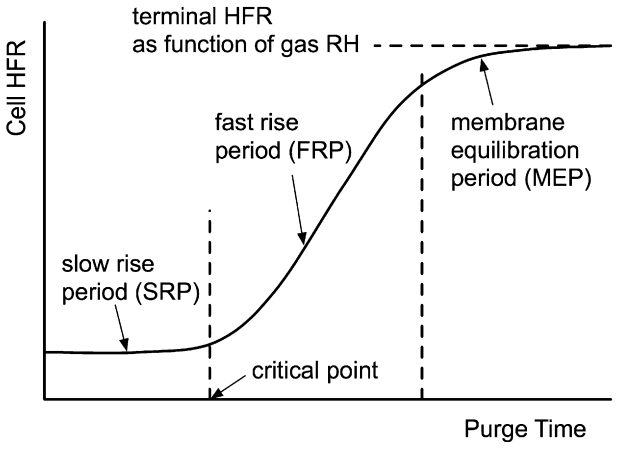

Fig. 3. Stages of purge curve.

3.2. Stages of purge

Fig. 2 also reveals general characteristics of a purge curve, consistent with the model prediction of Sinha and Wang [14]. Several stages of gas purge are evident from the 60-s purge case shown in Fig. 2. The first stage (between 0 and ~20 s) can be called the slow rise period (SRP) where the membrane HFR does not rise substantially. This stage can be subdivided into SRP1 (0 to ~10 s) and SRP2 (10 to ~20 s). Physically, SRP1 coincides with the through-plane drying where liquid water is evaporated from CL/GDL underneath the channel area. This is then followed by SRP2 where the drying front propagates along the in-plane direction into the land area [14]. During SRP1 and SRP2, the CL/GDL remains saturated with water vapor and hence the membrane remains nearly fully hydrated. We define the end of SRP as the critical point, at which contiguous clusters of liquid water have completely disappeared in CL/GDL. While the SRP seems ineffective to increase the membrane HFR, it is a required step of gas purge to clear liquid water from CL/GDL and every gas purge must go beyond the critical point to be effective. Thus, the critical point also defines the minimum purge duration.

After the critical point, purge enters the fast rise period (FRP) (between 20 and ~45 s in Fig. 2), where the membrane HFR is seen to rise substantially. Physically, the FRP coincides with the vapor diffusion process with the entire membrane subject to water desorption by dry gas. The FRP is finally followed by a membrane equilibration period (MEP) where water content in the membrane gradually reaches equilibrium with the relative humidity of purge gas. As a consequence, HFR asymptotically approaches the theoretical value corresponding to the equilibrium water content. In Fig. 2, due to the short duration of purge, the MEP is not clearly visible. A schematic illustration of all stages of gas purge is provided in Fig. 3. Evidently, the FRP is the most efficient period of gas purge. Hence, an optimized gas purge should pass beyond the critical point, take full advantage of the FRP, but not dwell on the MEP.

3.3. Effect of purge cell temperature

Based on our afore-mentioned hypothesis that the primary mechanism of water removal during gas purge is by the vapor phase, the purge performance is expected to strongly depend on the saturation vapor pressure or equivalently, the purge cell temperature. Figs. 4–6 show the purge curves and the final HFR after 60-s purge for various purge cell temperatures. The purge curves plotted in Fig. 4 correspond to three cell temperatures and two purge gases, respectively, with a constant flow rate of 4.5 L/min for each side. Two observations can be made. First, as the purge cell temperature increases, the HFR rise becomes faster and the final value at 60 s is higher. Second, at all temperatures the He purge is

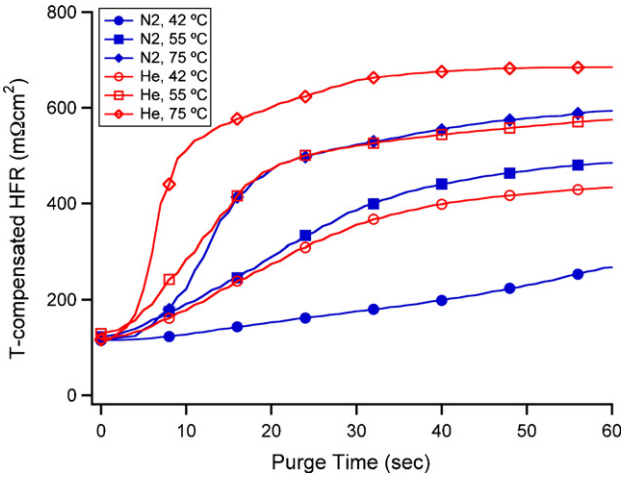

Fig. 4. Time evolution of cell HFR at different cell temperatures and for various purge gases. The purge gas flow rate was 4.5 L/min.

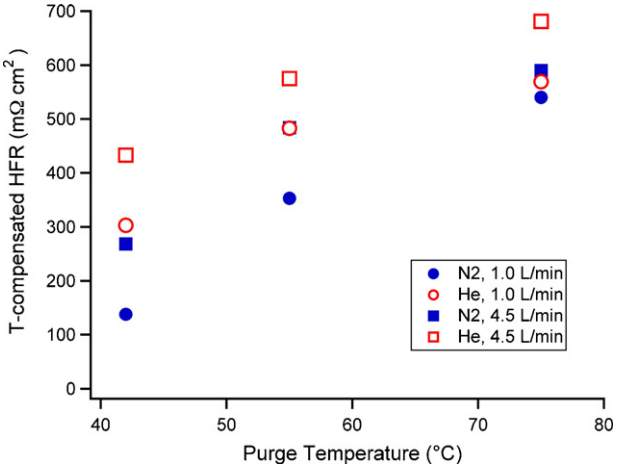

Fig. 5. Cell HFR after 60 s purge as a function of purge cell temperature.

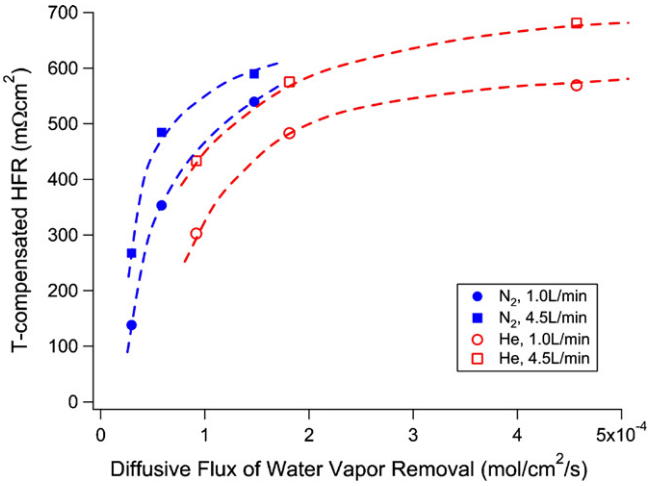

Fig. 6. Cell HFR after 60 s purge as function of diffusive flux of water vapor.

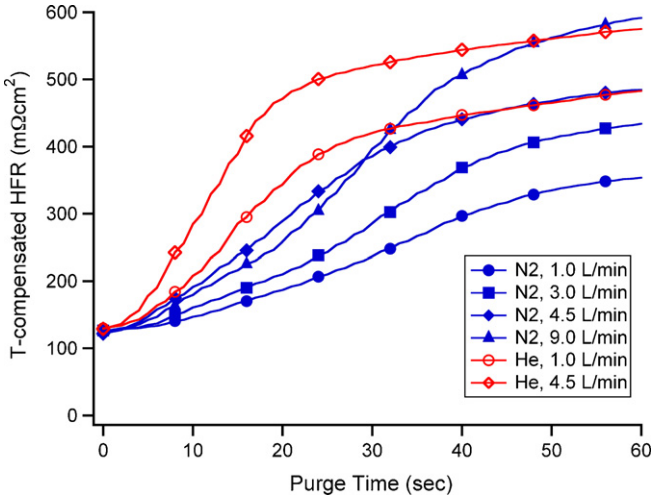

Fig. 7. Time evolution of cell HFR during purge at 55 °C cell temperature.

more effective than N_2. The final HFR value depends primarily on the slope of the FRP (between 5 and 10 s in He, 75 °C purge case, for instance) and this slope is related to the through-plane diffusive flux of water vapor. Furthermore, at 75 °C with He, the HFR approaches a constant asymptote of ~650 mΩ cm^2 already in less than 60 s, signifying the attainment of MEP of gas purge. From this result it can be expected that if all purge experiments continue for a sufficiently long period, the final temperature-compensated HFR values all approach ~650 mΩ cm^2.

In Fig. 5 the T-compensated HFR after 60 s purge is plotted as a function of temperature for two purge gases with two flow rates. At every temperature or flow rate, the He gas purge (open symbols) yields higher HFR than N_2 (solid symbols), due to its high water vapor diffusivity. However, with 1 L/min flow rate the advantage of He almost vanishes at 75 °C, as the water removal in this case is limited by the convective flux down the channel and the enhanced diffusion does not help.

Fig. 6 displays the T-compensated HFR as a function of the through-plane vapor diffusion flux. If there is sufficiently large flow rate, the resulting HFR should no longer be affected by the convective flux of water vapor down the channel, and hence the HFR would be determined only by the diffusive flux. In Fig. 6 it is seen that the purge curves for N_2, 1.0 L/min and He, 1.0 L/min deviate from each other even at the same diffusive flux (e.g. 1×10^{-4} mol/(cm^2 s)). This is because the flow rate in this case is not large enough to eliminate the effect of convective flux. Similarly, the purge curves for N_2, 4.5 L/min and He, 4.5 L/min differ, although the difference becomes smaller than the 1.0 L/min case, indicating that the contribution of convective flux becomes weaker at the higher flow rate. It is expected that if we further increase the flow rate, the purge curves for N_2 and He will collapse together over an entire range of the diffusive flux, indicative of a diffusion-controlled regime free of the convection effect down the channel.

3.4. Effect of purge gas flow rate

Next, the effect of the purge gas flow rate is studied and displayed in Figs. 7–9. The flow rate, or equivalently gas velocity, affects not only the vapor capacity rate of the channel flow but also the residence time of purge gas through the channels. The higher flow rate gas stays for a shorter time in the channel, allowing less vapor diffusion into the channel and reaching the exit with lower relative humidity, and vice versa. Therefore, even in the diffusion-

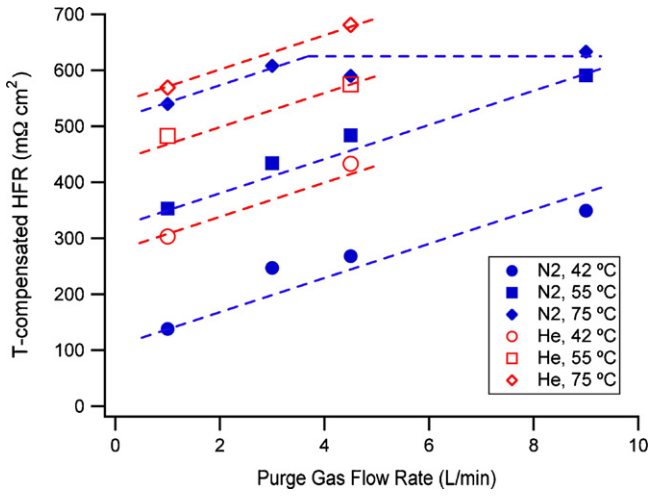

Fig. 8. Cell HFR after 60 s purge as function of purge gas flow rate.

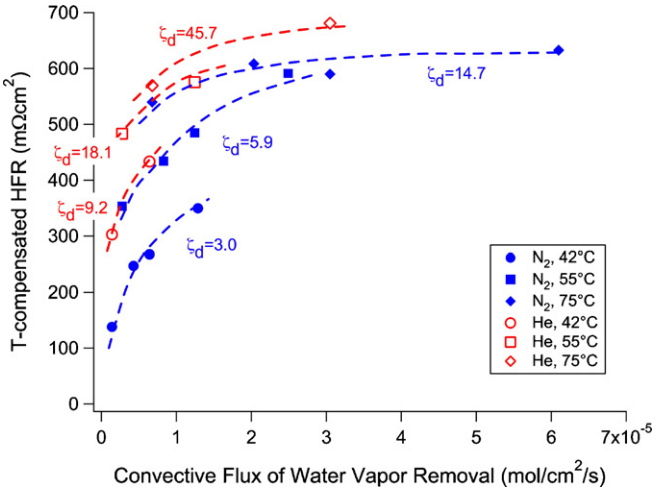

Fig. 9. Cell HFR after 60 s purge as function of convective flux of water vapor. ζ_d denotes the diffusion flux $\zeta_d = D(p_{v,sat} - p_{v,inlet})/RT/\delta_{GDL} \times 10^5$.

dominated regime the purge curve is partly controlled by the purge gas flow rate.

Fig. 7 shows the purge curves for various flow rates at 55 °C purge cell temperature. At a certain temperature (55 °C in this case) the slope of the HFR curve in the in-plane drying stage (i.e. SRP2) becomes larger, and the transition to the FRP takes place sooner for He than N_2. Larger flow rate results in the higher HFR rise for the aforementioned reasons. In Fig. 8 the T-compensated HFR is plotted as a function of purge gas flow rate for three different temperatures. In most cases the final HFR increases with the flow rate, but at 75 °C the final HFR of N_2 purge begins to level off at the flowrate of ~4 L/min and further increase in flowrate does not increase the HFR. It is believed that a regime controlled by through-plane vapor diffusion has been reached at this high temperature and high flowrate. Under the same conditions, the He gas purge is seen to yield higher HFR than N_2 because of its higher water diffusivity. In the diffusion-dominated regime or at the limit of sufficiently large flow rate, the rate of water removal is only determined by the diffusion parameter; as such, and the resulting HFR is higher for He purge than N_2.

It should be noted that the advantage of He gas purge diminishes with the increasing temperature, as can be seen from the purge curves displayed in Fig. 4. At high temperature such as 75 °C, the HFR evolution nearly reaches the equilibrium stage, in other words, the membrane is nearly equilibrated with the 40% RH purge gas after 60 s purge both in He and N_2 cases. However, the transition from FRP to MEP occurs much earlier for He gas purge (about 10 s at 75 °C) than for N_2 (about 20 s at 75 °C). Therefore, when the system requires the shorter purge duration such as 15 s, the advantage of He gas purge is still significant.

Next, the T-compensated HFR is plotted in Fig. 9 as function of the convective flux of water vapor down the channel, where the data points for the same diffusive flux are connected by a dashed line. It can be seen that all dashed lines corresponding to various diffusive fluxes do not cross each other and that at a certain convective flux the resulting T-compensated HFR value after 60 s purge monotonically increases with the diffusive flux. For instance, at the convective flux of 1×10^{-5} mol/(cm^2 s), the T-compensated HFR increases from 300 mΩ cm^2 at $\zeta_d = 3.0$ to 620 mΩ cm^2 at $\zeta_d = 45.7$. Thus, we conclude that the T-compensated HFR after 60 s purge may be expressed as a unique function of these two parameters only, namely:

$$\text{T-compensated HFR} = f\left(\frac{D(p_{v,\text{sat}} - p_{v,\text{inlet}})}{\text{RT}\,\delta_{\text{GDL}}}, \frac{Q(p_{v,\text{sat}} - p_{v,\text{inlet}})}{\text{RTA}}\right) \quad (2)$$

Eq. (2) is significant in that the HFR after purge becomes predictable based on calculations of the through-plane diffusive flux and convective flux down the channel.

3.5. Matching two parameters

To further test the hypothesis that the HFR after purge is uniquely determined by the two characteristic parameters defined above, two additional purge experiments were conducted as tabulated in Table 1 (cases # 19 and 20). In these experiments, both diffusive and convective fluxes are matched while the purge cell temperature is varied. Case # 2 (N_2, 55 °C, 1 L/min) has the parameters $(\zeta_d, \zeta_c) = (5.9, 2.8)$ while case # 19 (He, 42 °C, 2 L/min) has the parameters of (9.2, 2.9) which closely match case #2. Similarly, # 3 (N_2, 75 °C, 1 L/min) and #20 (He, 55 °C, 2.5 L/min) share the nearly identical diffusive and convective fluxes. The purge curves for these four cases with the diffusive and convective fluxes closely matched are displayed in Fig. 10. It is interesting to note that if the two characteristic parameters are matched, the HFR evolution indeed exhibits a similar pattern, and the resulting T-compensated HFR after 60 s purge is nearly equal. Fig. 10 strongly suggests that a purge curve can be adequately described by the diffusive and convective fluxes developed in this work.

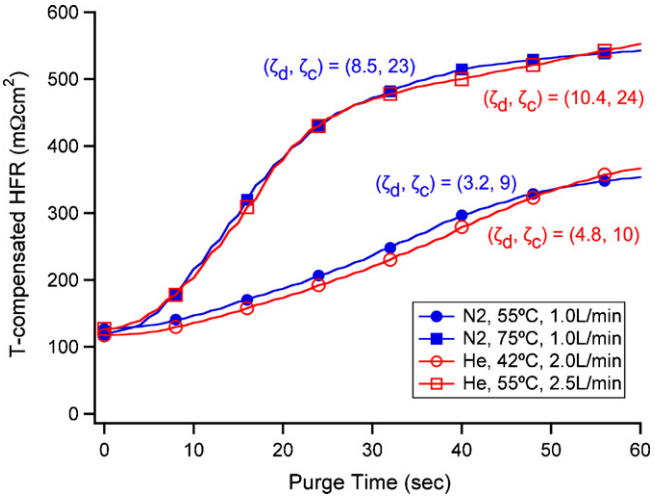

Fig. 10. Time evolution of cell HFR with matched parameters. ζ_d and ζ_c are the diffusion flux $\zeta_d = D(p_{v,\text{sat}} - p_{v,\text{inlet}})/RT/\delta_{\text{GDL}} \times 10^5$ and the convective flux $\zeta_c = Q(p_{v,\text{sat}} - p_{v,\text{inlet}})/RT/A \times 10^6$, respectively.

3.6. HFR relaxation

Another interesting phenomenon observed in this work is that after purge the cell HFR gradually decreases in a time scale of hours, which we call HFR relaxation after purge. Typical results of HFR relaxation are shown in Fig. 11. The purge conditions prior to the relaxation correspond to three different purge temperatures (42, 55, or 75 °C) with 4.5 L/min N_2 (cases #7–9 in Table 1). When the 60 s purge is completed, the valves at the inlet and outlet of the cell for both anode and cathode gas lines are closed and the cell temperatures are maintained constant at the purge cell temperature during the whole relaxation process.

Fundamental mechanisms of this relaxation phenomenon remain unknown and need future investigation. However, correlating the T-compensated HFR after relaxation with that after purge is of practical interest, because the initial membrane water

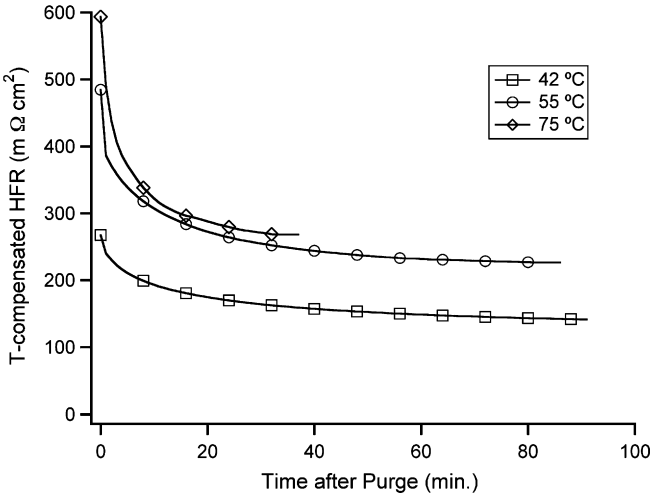

Fig. 11. HFR relaxation after purge.

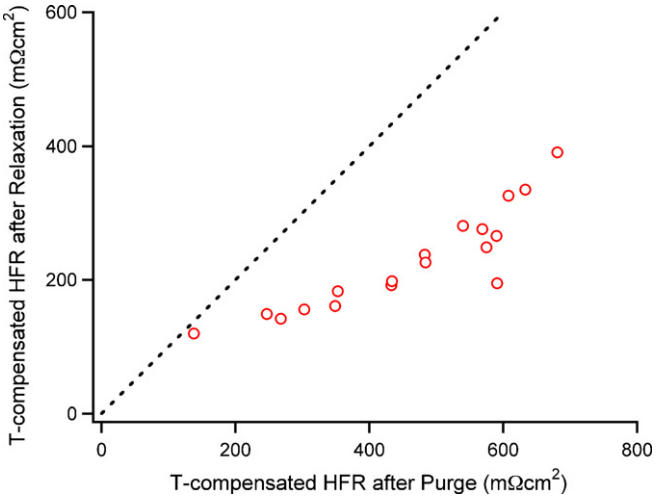

Fig. 12. Relation between HFR after relaxation and HFR after 60 s purge with purge gas RH greater than 40%. The dashed line symbolizes no HFR relaxation.

content critically important for PEFC cold-start performance corresponds to the HFR after relaxation (during cool-down), not the HFR immediately after purge. For this reason, we attempt an empirical correlation between the HFR after purge and that after relaxation, as shown in Fig. 12. It can be seen that a reasonable correlation exists over a range of HFR, or equivalently membrane water content, that ranges from full humidification to that corresponding to 40% RH. It is clear from Fig. 11 that the extent of HFR relaxation after purge increases with lowering membrane water content. Beyond the HFR corresponding to 40% RH, we do not include any data in Fig. 11 as they become widely scattered and somewhat chaotic. We note that HFR relaxation after purge becomes stochastically random as soon as the membrane becomes drier than that corresponding to 40% RH.

The correlation shown in Fig. 12 provides a practical means to estimate the HFR or membrane water content as the important input to evaluate cold-start performance [7,8]. That is, one can estimate the HFR after purge from Eq. (2) based on the purge conditions, and subsequently correct for HFR relaxation using Fig. 12. Based on the HFR value after relaxation or prior to cold start, one can use the analytical models and performance data developed in previous work [7,8] to estimate the cold-start performance.

4. Conclusions

We have described an experimental method to fundamentally investigate the performance of short-duration gas purge in PEFCs for the first time. This was made possible by development of a reliable purge experimental procedure with excellent repeatability. Specifically, the following conclusions are drawn from this study:

(1) A novel experimental procedure for gas purge studies is developed and its excellent repeatability is confirmed.
(2) A purge curve, defining the cell HFR versus purge time, can be generally categorized into the SRP controlled by through- and in-plane drying or liquid water removal from CL/GDL, the FRP characterized by vapor diffusion and significant membrane desorption of water, and the MEP where water content in the membrane asymptotically reaches equilibrium with relative humidity of purge gas.
(3) The end of the SRP is called the critical point. An optimal gas purge should pass beyond the critical point, take full advantage of the FRP, but not dwell on the MEP.
(4) Purge performance can be described by two parameters: the through-plane vapor diffusion flux from the CL/GDL to the gas channel, and the convective flux of water vapor along the channel with purge gas. The temperature-compensated HFR after gas purge is found to be predictable solely by these two parameters.
(5) There exists a unique correlation between HFR after relaxation and HFR after purge for the membrane water content down to that corresponding to 40% RH. This correlation thus enables the estimation of the membrane water content prior to cold start from the HFR after purge, which in turn can be calculated from the two characteristic parameters describing the purge process.

Finally, it is expected that the experimental procedure and method of analysis developed in this work are also applicable to other problems involving water removal from a polymer electrolyte fuel cell.

Acknowledgements

Funding for this work from Nissan Motor Co. Ltd. is gratefully acknowledged. We also thank JAPAN GORE TEX INC. for providing MEAs.

References

[1] S.-Y. Lee, E. Cho, J.-H. Lee, H.-J. Kim, T.-H. Lim, I.-H. Oh, J. Won, J. Electrochem. Soc. 154 (2007) B194.
[2] E.L. Thompson, J. Jorne, H.A. Gasteiger, J. Electrochem. Soc. 154 (2007) B783.
[3] E. Cho, J.-J. Ko, H.Y. Ha, S.-A. Hong, K.-Y. Lee, T.-W. Lim, I.-H. Oh, J. Electrochem. Soc. 151 (2004) A661.
[4] J. Hou, H. Yu, S. Zhang, S. Sun, H. Wang, B. Yi, P. Ming, J. Power Sources 162 (2006) 513.
[5] J. Hou, H. Yu, B. Yi, Y. Xiao, H. Wang, S. Sun, P. Ming, Electrochem. Solid-State Lett. 10 (2007) B11.
[6] X.G. Yang, Y. Tabuchi, F. Kagami, C.Y. Wang, J. Electrochem. Soc., in press.
[7] K. Tajiri, Y. Tabuchi, C.Y. Wang, J. Electrochem. Soc. 154 (2007) B147.
[8] K. Tajiri, Y. Tabuchi, F. Kagami, S. Takahashi, K. Yoshizawa, C.Y. Wang, J. Power Sources 165 (2007) 279.
[9] J. St-Pierre, J. Roberts, K. Colbow, S. Campbell, A. Nelson, J. New Mater. Electrochem. Syst. 8 (2005) 163.
[10] R. Bradean, H. Haas, A. Desousa, R. Rahmani, K. Fong, K. Eggen, D. Ayotte, A. Roett, A. Huang, Proceedings of the AIChE 2005 Annual Meeting, Cincinnati, OH, 2005.
[11] S. Ge, C.Y. Wang, Electrochim. Acta 52 (2007) 4825.
[12] P.K. Sinha, P. Halleck, C.Y. Wang, Electrochem. Solid-State Lett. 9 (2006) A344.
[13] J. St-Pierre, A. Wong, J. Diep, D. Kiel, J. Power Sources 164 (2007) 196.
[14] P.K. Sinha, C.Y. Wang, J. Electrochem. Soc. 154 (2007) B1158.